STUDIA UBB CHEMIA, LXV, 1, 2020 (p. 189-203)
(RECOMMENDED CITATION)
DOI:10.24193/subbchem.2020.1.15

MORPHO-TEXTURAL AND FLUORESCENCE STUDIES ON SiO_2 AND SiO_2@Ce^{3+}

ELENA-MIRELA PICIORUȘ[a], CĂTĂLIN IANĂȘI[a], ROXANA NICOLA[a], PAULA SFÎRLOAGĂ[b], PAULA SVERA[b], ANA-MARIA PUTZ[a]

ABSTRACT. Spherical silica xerogels were synthesized by Stöber route using tetra-ethyl-orthosilicate (TEOS) in order to obtain good properties for opto-electronic and catalytic applications. The reactants mole ratio was *n* TEOS: H_2O: ETOH: NH_3 (where *n* = 0.098 ÷ 0.26: 0.45: 0.789: 0.06). To study these properties, we know from literature, that nanoparticles under 100 nm show unique electrical, mechanical and optical properties. We have choosen the optimum sample, with the smaller surface area and particles size of 91 nm. To improve the optical properties, this sample was further doped with 0.1% Ce^{3+}. The obtained xerogel was thermally treated at 300, 600 and 900 ºC. The changes in properties were put in evidence by morpho-textural (N_2 adsorption–desorption isotherms and SEM images) and optical measurements (FT-IR, Fluorescence and Raman spectra's).

Keywords: *sol-gel, Ce (III) carbonate hydrate, Stöber, spherical particles*

INTRODUCTION

SiO_2 has been considered a promising material as host matrix for rare earth elements because of its transparence and simplicity in synthesis [1]. Generally, lanthanide ions, such as Ce^{3+} have been incorporated in SiO_2 matrix to tune the catalytic and fluorescence properties [2].

High annealing temperature of lanthanide doped nanomaterial's forming lanthanide ion clustering leading to the phase separation and the nanoparticles sintering have a reduction in surface area. As applications of these nanomaterial's, can be listed in optical domains, such as lasers [3] and as activators in SiO_2 materials because they allow 4f-5d optical transitions [4]. A. Vedda [5] observed that by increasing the concentration of Ce^{3+} above 0.1%, led to a decrease in fluorescence, due to the formation of aggregates or by valence changes.

[a] *"Coriolan Dragulescu" Institute of Chemistry, 24 Mihai Viteazu Bvd., 300223, Timisoara, Romania*
[b] *National Institute for Research and Development in Electrochemistry and Condensed Matter, 144 Prof. Dr. Aurel Paunescu Podeanu Str., Timisoara, Romania*
* *Corresponding author: putzanamaria@yahoo.com*

The sol-gel technique has the advantage over other methods because it yields materials with low density [6] this being an important factor for enhancing the fluorescence. The fluorescence of cerium doped SiO_2 may be influenced by multiple factors like modification of the ligand field around the Ce^{3+} ions in silica, presence of hydroxyl ions, energy transfer by cross relaxation and concentration of dopants [7]. Therefore, it is important to distinguish between the fluorescence ascending from Ce^{3+} ions and of that arising from defect centers in the silica matrix. In parallel to optical studies, structural and morphological investigation appeared to be useful, and the present work is specifically aimed at shedding further light on the incorporation of Ce^{3+} ions into the sol-gel silica matrix. The purpose of this study was to investigate the morphological and textural properties and to put in evidence the fluorescence by doping with 0.1% Ce^{3+} concentration and fired at three different temperatures.

RESULTS AND DISCUSSION

Firstly, the three xerogels obtained were characterized by physicochemical methods to underline the effect of TEOS concentration. In the second step we will effectively choose the optimum sample and we will add cerium as dopant to improve the fluorescent properties.

Part I

FT-IR Spectroscopy

Figure 1 shows the infrared transmission spectra of solid silica particles.

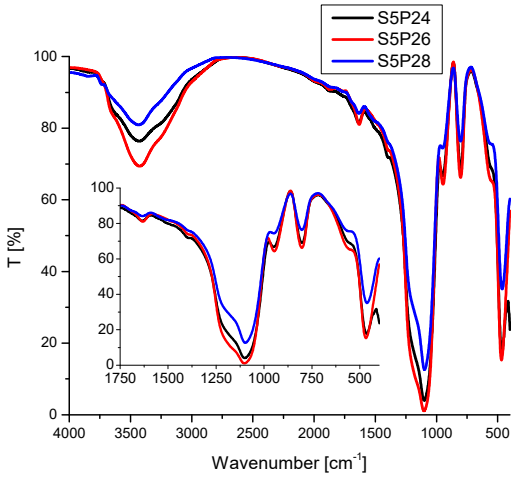

Figure 1. FT-IR spectra of dried (60 °C) silica xerogels with different [TEOS]

The broad absorption band around 3400-3600 cm^{-1} was assigned to stretching mode of the hydroxyl group and molecular water [8]. The peak at 1635 cm^{-1} can be ascribed to the H-O-H bending vibration of the free water or the physically absorbed water [9]. The absorption bands due to Si-OH stretching and bending vibrations appeared at ~950 cm^{-1} [10]. The spectrum reveals intense bands at 1100 cm^{-1}, 804 cm^{-1} and 468 cm^{-1} specific for Si-O-Si stretching, Si-O^- symmetric stretching and Si-O-Si asymmetric bending, respectively [9, 11]. The results indicate that all bands are suggesting the formation of a silica network.

N_2 adsorption - desorption isotherms

The textural parameters of dried silica xerogels, evaluated by N_2 adsorption - desorption isotherms are presented in **Figure 2**.

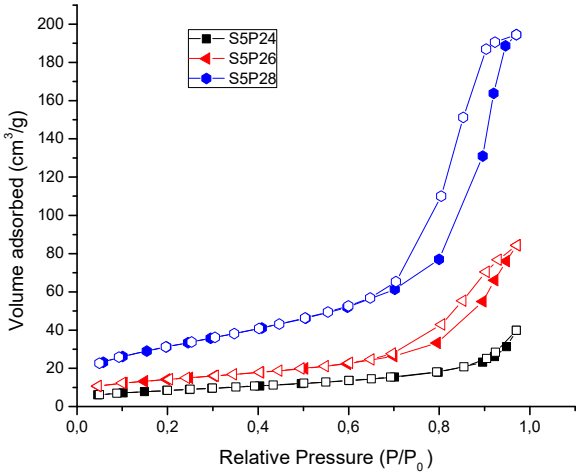

Figure 2. N_2 adsorption-desorption isotherms of dried xerogels

According to IUPAC classification [12, 13] the N_2 adsorption-desorption isotherms indicate for the sample with low TEOS concentration, S5P24, a *type II isotherms*, specific for non-porous materials. Also, this material presents a small percentage a type IVa isotherm with a type H3 hysteresis loop. With the increase of TEOS concentration, the N_2 isotherm of sample S5P26 indicate a *type IVa isotherms* which are characteristic for mesoporous materials presenting a H3 hysteresis loop specific for aggregates and slit-shaped pores [12, 13]. For xerogel S5P28, with the highest concentration of TEOS, exhibits a type IVa isotherm with a H1 hysteresis loop, typically characteristic for cylindrical pores [12, 13].

From N_2 adsorption-desorption isotherms, the textural parameters were evaluated and presented in Table 1.

Table 1. Textural parameters of silica xerogels with different TEOS concentrations

Xerogels	BJH Adsorption pore diameter [nm]	BJH Desorption pore diameter [nm]	BET surface area [m^2/g]	Total pore volume [cm^3/g]	Particle diameter* [nm]
S5P24	3.63	3.03	29.8	0.061	91
S5P26	15.22	8.94	49.2	0.013	55
S5P28	15.32	9.03	112.8	0.030	24

**Particle diameter was calculated with the: ($D_{particle}$) = 6/Ssp*d_{SiO2}*10^6*

In Figure 3 *the pore size distribution* was assessed from N_2 adsorption-desorption isotherms, using the method proposed by Barrett, Joyner and Halenda (BJH) [14]. The sample S5P26 and S5P28 indicate a wider unimodal pore distribution in the range of 10-20 nm. For xerogel S5P24 the pore size distribution indicates a very small diameter of pore with less than 4 nm.

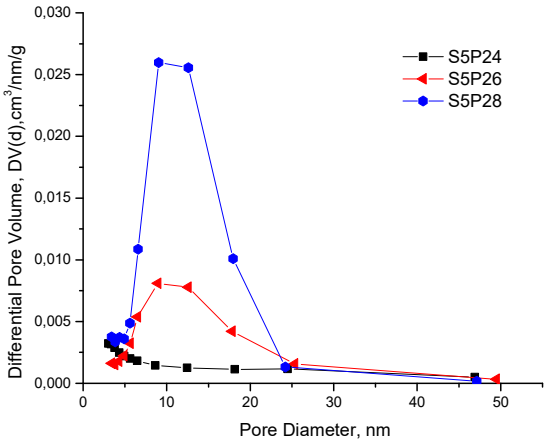

Figure 3. Pore size distribution

The particle sizes were calculated with the equation proposed by Sun et al. [15]. It was observed that the size of particles decreases with the increase of TEOS concentration. The decrease of particle size below 100 nm enables good optical transparency, especially for silica [16].

The sample S5P28, with the maximum concentration of TEOS, presented the highest surface area value with a value of ~113 m2/g.

SEM

The morphology of the silica xerogels was evaluated by Scanning Electron Microscopy (SEM) and the SEM images are shown in Figure 4.

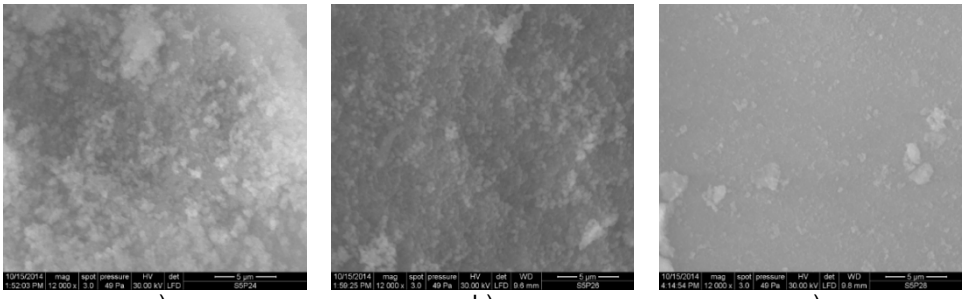

a) b) c)

Figure 4. SEM image of xerogels: a) S5P24 TEOS 0.098M, b) S5P26 TEOS 0.179M and c) S5P28 TEOS 0.26M.

From Figure 4 it was observed that the amount of TEOS is very important to control the size of particles and morphology. It can be seen that by varying the TEOS concentration in the range 0.098-0.26M has a major impact on the morphology of silica xerogels. Correlating the data from SEM images with N_2 adsorption-desorption isotherms we observed that as the amount of TEOS is increased above 0.098 M TEOS to 0.26M TEOS, the silica nanoparticles decrease in diameter ranging from 91 nm to 24 nm in diameter. The morphology for all samples indicates spherical shape. In case of sample S5P24 more irregular clusters are formed but in case of sample S5P28 the surface is smoother.

Fluorescence spectra

The Figure 5 a), b) shows the emission spectra in the range of 525-750 nm, at a rate of 100 nm/min, of samples excited at 433 nm and 480 nm with the slit width of 10 nm for excitation and 7.5 nm for emission.

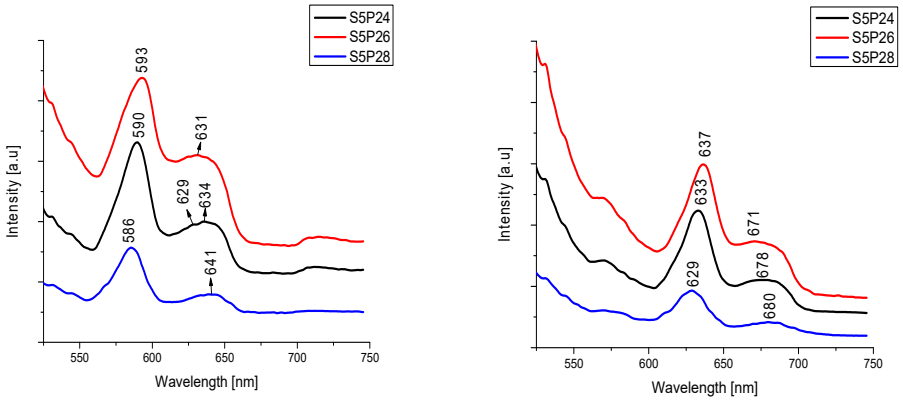

a) b)

Figure 5. Fluorescence image of silica nanoparticles a) excited at 433 nm b) excited at 480 nm

For sample excited at 433 nm the spectra indicate two main emission peaks at ~590 nm and ~635 nm. For sample excited at 480 nm the spectra present two main peaks at ~630 nm and 680 nm. With the increase of TEOS concentration the spectra reveal a bathochromic effect and by increasing more the quantity of TEOS a hypsochromic effect occurs. The shifts in all samples are almost the same. The sample S5P26 present the best fluorescence properties in both cases. Correlating our results with the literature we observed that all shifts and fluorescence properties of the samples are due to defects in structure formation.

Raman spectra

By using Raman spectroscopy, the three xerogels dried at 60 °C with different TEOS concentration were evaluated and presented in Figure 6.

The results from Raman spectroscopy correlated with FT-IR spectra indicate for all samples a rather weakly developed peak situated at 435 cm^{-1} corresponding to siloxane ring breathing mode (with 3 or 4 SiO^- units) [17, 18] or to bending vibrations in Si-O-Si bridges [19, 20]. Comparing the data with fluorescence spectra the results showed that the intensity of fluorescence is changing, the most prominent fluorescence is observed in the case of S5P26, followed in decreasing order by S5P28 and S5P24.

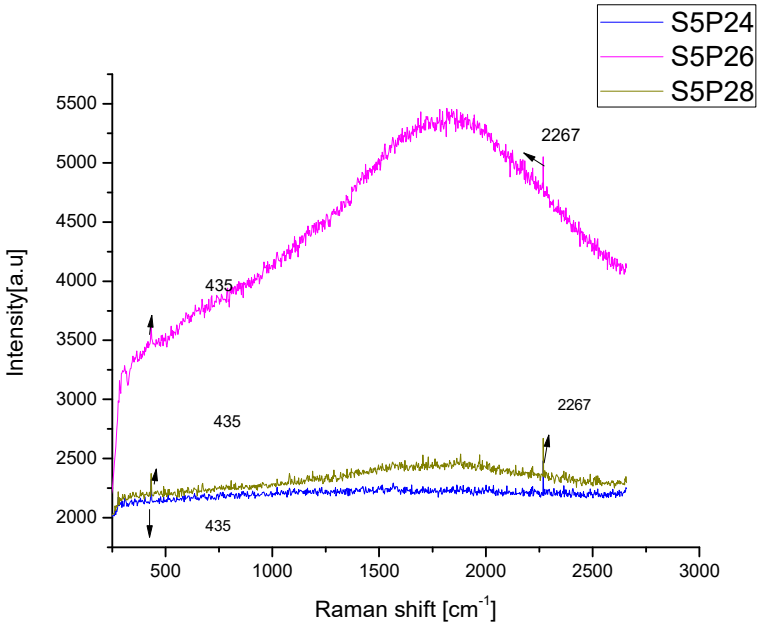

Figure 6. Raman spectra of xerogels dried at 60 °C

The material with required properties was further doped with cerium in order to improve the fluorescence. Based on the results, the sample S5P24 was chosen due to small surface area and higher particle size.

Part II

In this second part, the selected material, S5P24 was doped with 0.1% Ce^{3+} concentration and thermally threated at 3 different temperatures (300, 600 and 900°C).

FT-IR Spectroscopy

The FT-IR spectra of the blank xerogel sample S5P24 with 0.1% Ce concentration dried at 60°C and fired at three different temperatures are shown in Figure 7.

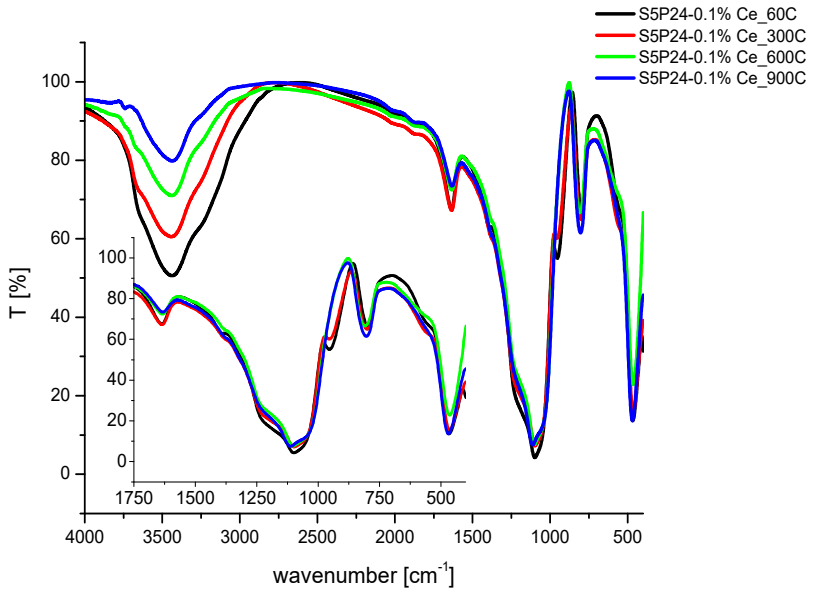

Figure 7. FT-IR spectra of xerogel S5P24 with 0.1% Ce^{3+} concentration dried at 60°C and treated at different fired temperature

After the cerium was added, the broad band at ~3440 specific for the –OH symmetric stretching from the surface hydroxyl group was observed [21]. By increasing the temperature, the bands specific to -OH are decreasing in intensity. Similar behavior can be seen for the bands at 1634 cm^{-1}, possible due to the existence of residual free water resided in the pores of the xerogel. From Figure 7, the specific bands of silica at ~1100 cm^{-1}, ~800 cm^{-1} and ~470 cm^{-1} were observed. With the increase of temperature, the intensity of bands is more increased indicating the formation of $[SiO_4]^{4-}$ tetrahedral units and Si-O-Si bonds [22, 23]. After thermal treatment at 300 °C, the Si-OH bonds observed at ~950 cm^{-1} starts to brake and above 600 °C the bands are disappeared due to decomposition of hydroxyl group. Due to small quantity of cerium introduced in synthesis of 0.1% Ce concentration, the bands specific are overlapped with the silica bands.

N_2 adsorption desorption isotherms

The textural parameters of xerogels with 0.1% Ce concentration dried at 60°C and thermally threated at three temperatures was evaluated by N_2 adsorption -desorption isotherms and are presented in Figure 8.

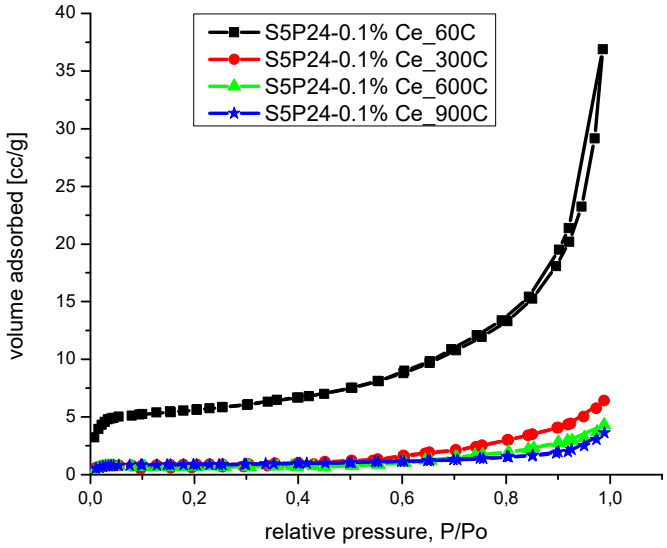

Figure 8. N_2 adsorption-desorption isotherms of xerogels with 0.1% Ce concentration dried at 60°C and fired at 300, 600 and 900 °C

From Figure 8, according to IUPAC we can assume that sample S5P24-0.1% Ce_60C indicate a type IVa isotherm with a hysteresis of H3 but in case of the fired sample the isotherms are type II isotherms. The textural parameters obtained are presented in Table 2.

Table 2. The textural data of sample S5P24 with 0.1% Ce concentration dried at 60 °C and fired at 300, 600, 900 °C

Xerogels	BJH Adsorption pore diameter [nm]	BJH Desorption pore diameter [nm]	BET surface area [m^2/g]	Total pore volume [cm^3/g]
S5p24-0.1% Ce_60C	5.670	4.965	22.6	0.057
S5p24-0.1%Ce_ 300C	4.936	4.891	4.2	0.010
S5p24-0.1%Ce _600C	4.965	4.951	4.0	0.007
S5P24-0.1%Ce_900C	3.853	3.297	3.5	0.006

In Figure 9 the pore size distribution obtained by BJH method was presented.

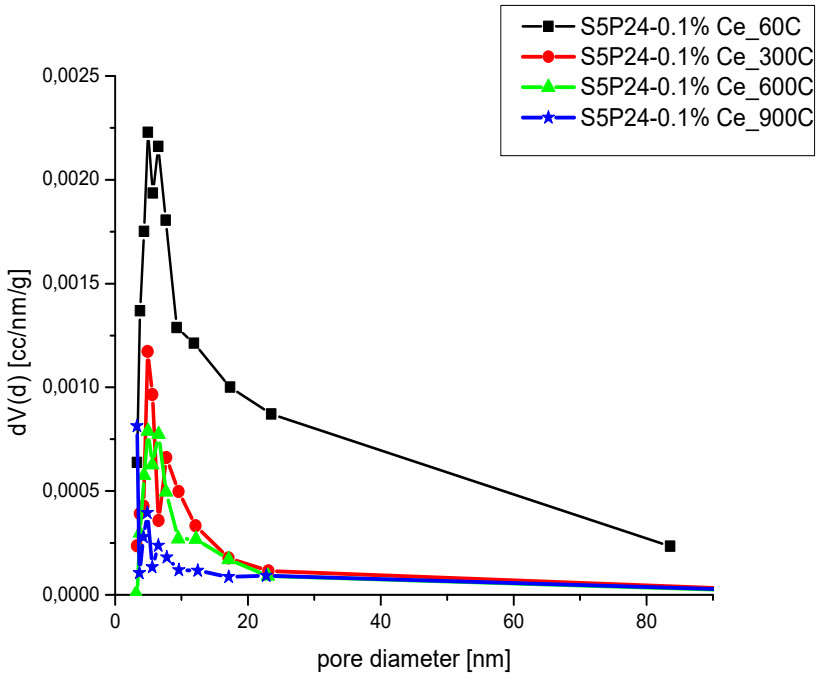

Figure 9. Pore size distribution of xerogel sample S5P24 with 0.1% Ce concentration dried at 60°C and fired at 300, 600 and 900 °C

Evaluating the results obtained we can conclude that, with the increase of temperature, the pore size distribution, surface area and total pore volume is decreasing indicating that the skeletal structure of silica shrinks.

Fluorescence spectra

Figure 10. a), b) shows the emission spectra of nanocomposites with cerium in the range of 525-750 nm, at a rate of 100 nm/min, of samples excited at 433 nm and 480 nm with the slit width of 10 nm for excitation and 7.5 nm for emission.

From Figure 10, by overlapping the emission bands, it has been observed that after fired the sample above 300 ^{o}C the intensity decreases because of pore collapsing [24].

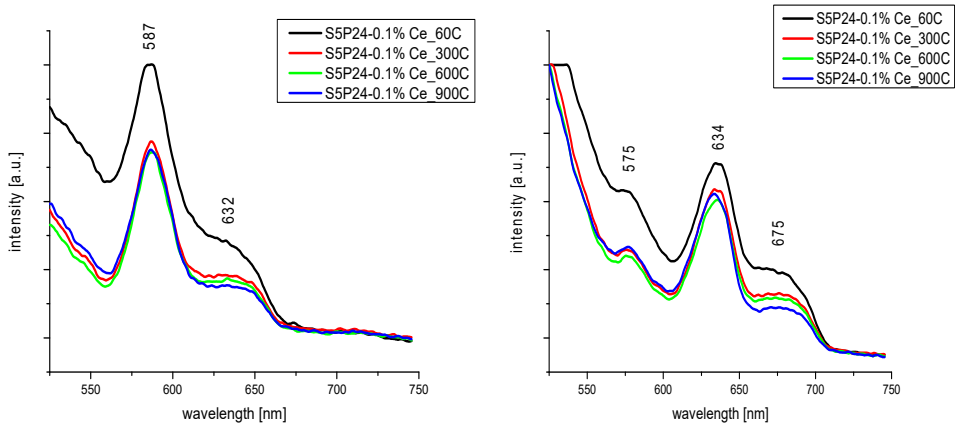

a) b)

Figure 10. The S5P24@0.1%Ce^{3+} dried at 60 °C and S5P24@0.1%Ce^{3+} series of samples fired at 300, 600 and 900 °C, a) Excitation at 433 nm and b) Excitation at 480 nm

For sample excited at 433 nm, the cerium nanocomposites indicate a small hypsochromic effect for the maximum at 593 nm in case of silica doped cerium and dried at 60°C. In case of sample excited at 480 nm, the cerium nanocomposites indicate no shifts in spectra.

Raman spectra

Figure 11 represent the Raman spectrum of S5P24 sample with 0.1% Ce concentration dried at 60°C and fired at 300, 600 and 900 °C.

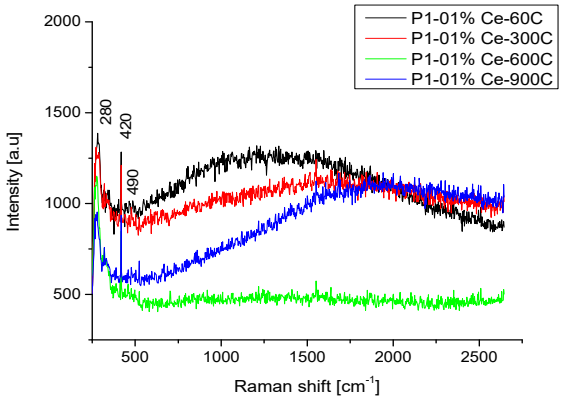

Figure 11. RT Raman spectra of S5P24@0.1%Ce^{3+} dried at 60 °C and S5P24@0.1%Ce^{3+} fired at 300, 600 and 900 °C

The CeO_2 exhibits a strong band at 462 cm^{-1} due to F_2g Raman active mode. This bands corresponds to the triply degenerate F_2g mode and can be viewed as a symmetric breathing mode of the oxygen atoms around cerium ions [25]. Also, from literature, the Ce-O stretching vibrations at 402 and 490 cm^{-1}, were found in cerium (II) oxide-hydroxide [26] In our case, the Raman spectra obtained shown a prominent band at 420 cm^{-1} meaning that cerium is present. Also, the Raman features of SiO_2 are observed at 490 cm^{-1} assigned to symmetric stretching modes of four-fold and three-fold rings of SiO_2 tetrahedra [27].

Besides, it also exhibits a prominent 280 cm^{-1}, which are attributed respectively to the normal Raman inactive (IR active) transverse and longitudinal optical photon modes at the Brillouin zone center (IR active) transverse and longitudinal optical photon modes at the Brillouin zone center [28].

CONCLUSIONS

Spherical silica particles were synthesized by sol-gel process, Stöber method. In this paper, was investigated how the precursor concentrations (TEOS) from 0.049 to 0.26 M TEOS affected the characteristics of the synthesized silica powders. Also, the fluorescence properties on the sample S5P24, with the lowest degree of fluorescence intensity, doped with 0.1%Ce^{3+} and fired at three different temperatures, were studied. For xerogels samples dried at 60°C, the FT-IR spectra has showed the main specific bands for silica. From morpho-textural properties, for the sample S5P28 (0.26M) the highest pores diameter (9 nm from N_2 desorption branch isotherm), and surface area (113 m^2/g) were obtained. The spherical shape of the silica particles was due to ammonia, which acts as catalyst in Stöber process. From fluorescence spectra, by exciting the samples at two different wavelengths 433 nm and 480 nm, the best fluorescence properties for sample S5P26 were registered. From Raman spectroscopy, the prominent fluorescence also for sample S5P26, and the lowest intensity of fluorescence for sample S5P24 were showed. To improve the fluorescence, the sample S5P24 was co-doped with 0.1% Ce^{3+} concentration. Sintered at three different temperatures (300, 600, 900°C), the morpho-textural and fluorescence properties were investigated. By increasing the temperature, the surface area, pore size distribution and total pore volume were decreased. From FT-IR spectra, the bands specific for Ce^{3+} are overlapped with the silica bands. The fluorescence spectra exhibited an increase in fluorescence intensity for xerogel sample S5P24 doped with 0.1% Ce^{3+} concentration. The Raman spectra has shown that the band situated at 420 cm^{-1} validated the Ce^{3+} appearance. In

conclusion, the major differences are observed in the obtained intensities of the spectra, in which case the samples doped with cerium have the highest intensity and therefore, superior fluorescence properties.

EXPERIMENTAL

Reagents

*Tetra-ethyl-orthosilicate (TEOS, 98% Merck), absolute ethanol (ETOH, 99.8%, Riedel de Haën), ammonia (NH_3, 25%, S.C. Silal Trading SRL); $Ce_2(CO_3)_2$*xH_2O.*

Synthesis

Three silica xerogels samples were synthesized by sol-gel technique using different molar ratios TEOS as silica precursor and NH_3 as alkaline catalyst.

In a 150 mL Berzelius glass, was added 10.5 mL ammonia solution of 12.5% concentration was added in 42 mL ethanol. The solution was mechanically stirred ten minutes at ±50°C and 400 rot/min. After ten minutes, were added different amounts of TEOS (22, 40, 60 mL) and, the solution became opaque and precipitate, being left five hours to be mechanically stirred. The silica particles were centrifuged and washed with water and ethanol four times. The decanted solution was dried at the oven at 60°C for 12 hours. In Table 3 and Table 4 it has presented the mole and amount of each reactants utilized in obtained of spherical silica xerogels.

Table 3. Xerogel's synthesis parameters

Xerogels	TEOS [Mol]	H_2O [Mol]	ETOH [Mol]	NH_3 [Mol]	$NH_{3solution}$[%]
S5P2-4	0.098	0.45	0.789	0.06	12.5%
S5P2-6	0.179	0.45	0.789	0.06	12.5%
S5P2-8	0.260	0.45	0.789	0.06	12.5%

Table 4. Amounts of reactants

	S5P2-4	S5P2-6	S5P2-8
TEOS [mL]	22	40	60
ETOH [mL]	42	42	42
$NH_{3solution}$ 12.5%[ml]	10.5	10.5	10.5

Synthesis of S5P24@Ce^{3+}

Silica doped with Ce^{3+} ions were synthesized by sol-gel technique using TEOS, ETOH, 12.5%NH_3 as catalyst, Ce(III) carbonate hydrate 99%, $Ce_2(CO_3)_{3*}xH_2O$ as material sources. During the preparation of silica nanocomposite, 42 mL ETOH was mixed in a beaker of 150 mL with 12.5% dilute aqueous NH_3 solution (10.5 mL). The solution was mechanically stirred at ±50°C, 400 rpm for 10 min. After that, the 0.009 g of Ce (III) carbonate were added in the solution with 0.1% Ce^{3+} concentration and the solution was stirred 30 minutes. To ensure the hydrolysis and condensation reactions, 22 mL TEOS was added and the mixture was stirred for 5 hours at ±50°C (400 rpm). Then, the gels were washed with distilled H_2O and ETOH four times, centrifuged and dried at 60°C (12 hours). Then, the nanocomposite was calcined at 300°C, 600°C and 900°C.

Characterization

BET (Brunauer-Emmett-Teller) technique was used to determine the surface area; BJH (Barrett-Joyner-Halenda) was used for determining the pore diameter; the both methods were determined from N_2 adsorption-desorption isotherm by using a Quantachrome Nova 1200e. Size and morphology of samples were determined by Field Emission Scanning Electron Microscopy, (*SEM)*. For SEM an INSPECT S (FEI Company, Holland) instrument has been used. FT-IR spectra were carried out as KBr pellets, in the 4000-400 cm^{-1} range on JASCO 430 apparatus and the fluorescence has been measured with the Perkin Elmer spectrophotometer. Raman spectra was done with Shamrock 500i Spectrograph from Andor United Kingdom.

ACKNOWLEDGMENTS

The authors thank to Romanian Academy for the financial support: Program 4. *Inorganic compounds and hybrids with relevance in nanostructured materials science, precursors for advanced materials.*

REFERENCES

1. O. M. Ntwaeaborwa; P. H. Holloway; *Nanotechnology*, **2005**, *16(6)*, 865–868.
2. R.S. Ningthoujam; V. Sudarsan; A. Vinu; P. Srinivasu; K. Ariga; S.K. Kulshreshtha; A.K. Tyagi; *J. Nanosci. Nanotechnol.* **2008**, *8(3)*, 1489-1493.
3. R. Reisfeld; *Opt. Mater.*, **2001**, *16(1-2)*, 1-7.
4. V. P. Dotsenko; I. V. Berezovskaya; N. P. Efryushina; A.S. Voloshinovskii; P. Dorenbos; C. W. E van Eijk; *J. Lumin.*, **2001**, *93(2)*, 137-145.

5. A. Vedda; A. Baraldi; C. Canevali; R. Capelletti; N. Chiodini; R. Francini; M. Martini; F. Morazzoni; M. Nikl; R. Scotti; G. Spinolo; *Nucl. Instrum. Methods Phys. Res. A.;* **2002**, *486(1-2)*, 259–263.
6. W. Stoeber; A. Fink; E. Bohn; *J. Colloid. Interface. Sci.*, **1968**, *26(1)*, 62-69.
7. A. J. Silversmith; N. T. T. Nguyen; B. W. Sullivan; D. M. Boye; C. Ortiz; K.R. Hoffman; *J. Lumin.*, **2008**, *128*, 931–933.
8. C. J. Brinker; G. W. Scherer; *Sol-Gel Science, The Physics and Chemistry of Sol-Gel Processing, Academic Press*: New-York, **1990**; pp. 581-585.
9. A Beganskienė; V. Sirutkaitis; M. Kurtinaitienė; R. Juškėnas; A. Kareiva; *Mater. Sci.*, **2004**, *10(4),* 287-290.
10. C. L. D. Vasconcelos; W. R. Campos; V. Vasconcelos; W. L. Vasconcelos; *Mater. Sci. Eng. A-Struct.*, **2002**, *334(1-2)*, 53-58.
11. A. Bertoluzza; C. Fagnano; M. A. Morelli; V. Gottardi; M. Guglielmi; *J. Non-Cryst. Solids*, **1982**, *48(1)*, 117-128;
12. K. S. W. Sing; D. H. Everett; R. W. Haul; L. Moscou; R. A. Pierotti; J. Rouquerol; T. Siemieniewska; *Pure Appl. Chem., **1984***, *57*, 603–619.
13. M. Thommes; K. Kaneko; A. V. Neimark; J. P. Olivier; F. Rodriguez-Reinoso; J. Rouquerol; K. Sing; *Pure Appl. Chem.*, **2015**, *87(9-10),* 1051-1069.
14. E. P. Barrett; L. G. Joyner; P. P. Halenda; *J. Am. Chem. Soc.*, **1951**, *73(1)*, 373-380.
15. S. Sun; H. Zeng; *J. Am. Chem. Soc.,* **2002**, *124*, 8204–8205.
16. I. A. Rahman; P. Vejayakumaran; C.S. Sipaut; J. Ismail; C.K. Chee; *Mater. Chem. Phys.*, **2009**, *114(1)*, 328–332.
17. H. Zhang; D. R. Dunphy; X. Jiang; H. Meng; B. Sun; D. Tarn; M. Xue; X. Wang; S. Lin; Z. Ji; R. Li; F. L. Garcia; J. Yang; M. L. Kirk; T. Xia; J. I. Zink; A. Nel; C. J. Brinker; *J. Am. Chem. Soc.*, **2012**, *134(38)*, 15790−15804.
18. L. Brentano-Capeletti; J. H. Zimnoch; Fourier Transform Infrared and Raman Characterization of Silica-Based Materials, in *Applications of Molecular Spectroscopy to Current Research in the Chemical and Biological Sciences*, M. Stauffer Eds.; Intech Open, London, UK, **2016**, Chaper 1, pp. 3-21.
19. P. Borowicz; A. Taube; W. Rzodkiewicz; M. Latek; S. Gieraltowska; *Sci. World J.,* **2013**, *2080-2081,* 1-6.
20. K. J. Kingma; R. J. Hemley; *Am. Mineral.* **1994**, *79(3-4),* 269-273.
21. Y. Li; X. Yu; T. Yu; *J. Mater. Chem. C*, **2017**, ***5***, 5411-5419.
22. I. Coroiu; E. Culea; A. Darabont; J. *Magn. Magn. Mater.*, **2005**, *290-291*, 997–1000.
23. Y. Yu; D. Chen; Y. Wang; W. Luo; Y. Zheng; Y. Cheng; L. Zhou; **2006**, *Mater. Chem. Phys. 100(2-3),* 241–245.
24. A. Papavasiliou; D. Tsiourvas; E. G. Deze; S. K. Papageorgiou; F. K. Katsaros; E. Poulakis; C. J. Philippopoulos; N. Boukos; Q. Xin; P. Cool; *Chem. Eng. J.* **2016**, *300*, 343–357.
25. X. M. Lin; L. P. Li; G. S. Li; W. H Su; *Mater. Chem. Phys.*, **2001**, *69(1-3)*, 236-240.
26. F. Liu; L. Chen; J. K. Neathery; K. Saito; K. Liu; *Ind. Eng. Chem. Res.* **2014**, *53*,16341-16348.
27. A. Pasquarello; R. Car; *Phys. Rev. Lett.*, **1998**, *80(23)*, 5145-5147.
28. J. Z. Shyu; W. H. Weber; H. S. Gandhi; *J. Phys. Chem.,* **1988**, *92(17)*, 4964-4970.